ingegneria sismica
International Journal of Earthquake Engineering
Anno XLIII - Num. 1 - 2026

A low-complexity precoding detection algorithm for non-circular signals in the 230 MHz band in highly concurrent environments

Qiusheng Gao[1], *Jiaju Zhang*[1,*], *Xianglong Meng*[1], *Sinuo Jiao*[1] *and Junpeng Zhang*[1]

[1] State Grid Hebei Electric Power Company Co. Ltd Information & Telecommunication Branch, Shijiazhuang, Hebei, 050000, China

SUMMARY: *MIMO system in wireless communication refers to the technique of wireless transmission using multiple transmitte r and receiver antennas. The study focuses on MIMO systems in 230 MHz band in high concurrency environments and gives low complexity solutions based on enhancement at the transmitter side and optimization at the receiver side. The Lattice Base Lumped Simplicity (LLL) algorithm is combined with the V-BLAST ordering mechanism at the transmitter side. Inter-user interference is suppressed by matrix orthogonalization and optimal transmitter layer ordering. At the receiver side, the statistical properties of non-circular signals such as BPSK are mined to systematically derive the extended ZF (EZF) and extended MMSE (EMMSE) detectors. These two detectors effectively separate the signal and interference by constructing the augmented signal model. In a 2x2 MIMO system, the Gergely Simplified + V-BLAST scheme saves about 4-6 dB of transmit power compared to linear precoding at BER=0.01. At 10dB SNR, the LLL+V-BLAST user-reachable rate reaches 7.612bit/s/Hz, which is 1.07 times of the spherical lattice decoding, while its computational complexity is only 54.72% of SD. Under the condition of overload factor β=1.5 and number of antennas 130, the total rate of ML detection is 331 bit/s/Hz.EMMSE reaches 341 after 3 iterations and even exceeds ML.*

KEYWORDS: *mimo system; noncircular signals; precoding detection; lattice basis approximation; extended MMSE*

1 Introduction

At present, the power communication network mainly uses GPRS, CDMA, 3G/LTE, xPON fiber, power line carrier, industrial switch, 230 MHz wireless private network and other technologies, but from the effect of the current operation of the power grid companies around the world, due to the need to consider the site conditions, application requirements, economic costs and other factors, there is no one communication method can completely solve the full coverage of the power communication network problem [1]. Although the application of terrestrial fiber optic and cellular network has formed a large scale, but the terrestrial network is limited by the coverage of fiber optic laying and cellular base stations, many geographically remote and island areas, there is no terrestrial fiber optic and cellular network coverage, there is still a “gap” in the communication problem [2, 3]. Moreover, terrestrial networks are also affected by natural disasters such as earthquakes and floods. In addition, it has been shown that the channel conflicts caused by a large number of terminals communicating at high concurrency and the limited parallel demodulation capability have resulted in the number of concurrent terminals that can be supported by the power communication network being far from being able

*jiajuzhang2025@163.com
https://doi.org/10.65102/is2026230
Published: 30 April, 2026

to meet the demands of highly concurrent environments (e.g., complex smart distribution network scenarios) [4].

The concurrent communication capability between terminals and gateways of existing power communication networks cannot meet the application requirements of large-scale power distribution networks, which is mainly due to channel conflicts caused by the concurrent transmission of a large number of terminal devices. Aiming at the high concurrency environment, Cuomo, F et al. proposed the EXP LoRa-SF algorithm based on the distance/RSSI measurement and the total number of connected devices for selecting the appropriate SF (spreading factor) for the terminal devices in response to the problem of how to efficiently allocate channel resources to guarantee the concurrent communication of a large number of terminal devices and further proposed the EXP LoRa-AT algorithm for allocating the SFs for each terminal, so that packet over-the-air transmission time of each SF packet is the same throughout the network [5]. Reynders, B et al. proposed a two-step lightweight scheduling method (RS-LoRa) which is able to capture the effect impact in high concurrency environments leading to a large number of transmission conflicts, simulation experiments show that the method reduces the packet loss rate by 20% and improves the system throughput and fairness with 1000 end nodes [6]. Gamage, A et al. proposed an efficient Carrier Listening Multiple Access Technique (LMAC) for long-distance transmission for highly concurrent environments, which utilizes CAD techniques to listen to the occupancy of the relevant channels before packets are sent in order to mitigate the probability of packet conflicts on the specified CF (Carrier Frequency)/SF channels and to balance the load on each channel [7]. Lyu, J et al. In order to efficiently allocate channel resources to support large-scale concurrent terminal communications while solving the problem of distance and proximity effects brought about by the decentralized deployment of terminal devices, a joint SF allocation, TP control, and transmission duty cycle regulation strategy based on the average channel statistics and the spatial distribution of terminals is proposed to maximize the minimum throughput rate of all nodes [8]. El-Aasser, M et al. In order to solve the problem of assigning SFs to support a large number of terminals communicating concurrently, they proposed two methods to adjust the coverage of each SF by customizing the CR (coding rate) and SF parameter methods, and the proposed algorithms aim to maximize the throughput rate of each SF to improve the performance of the whole network [9]. Kouvelas, N et al. proposed a p-CSMA based MAC layer protocol to address the problem of severe transmission conflicts when large-scale terminals are communicating in parallel, and performance evaluation on the NS-3 simulation platform confirmed that the method significantly improves the packet delivery success rate [10].

In communication systems, the high number of antennas makes all-digital precoding too costly and difficult to implement, so hybrid precoding techniques, which incorporate digital and analog precoding, have arisen. Hybrid precoding technique is an important signal processing method to increase the channel capacity and reduce the inter-signal interference, and can achieve good communication system performance while reducing the hardware cost. Regarding the study of hybrid precoding technique, Shaban, A W et al. designed a hybrid precoding algorithm based on auxiliary candidate vector codebook by calculating the threshold value of channel mutual information and constructing precoding matrix by searching from weighted statistical candidate vector codebook with the threshold value as the target, which has a good spectral performance and low channel feedback overhead [11]. Dai, L et al. designed a hybrid precoding scheme based on continuous interference cancellation to decompose the performance maximization problem into a finite number of subantenna array performance maximization problem to obtain the optimal digital and analog precoding matrices to improve the spectral efficiency of the system [12]. Cui, M and Zou, W design the precoder and combiner through the equivalent channel, which is firstly transformed into the maximized equivalent channel

problem, and then based on the alternating optimization method, the design of the analog precoder and combiner is completed through iteration, and then the equivalent channel matrix is processed by SVD to complete the solution of the digital precoder and combiner [13]. Guo, Y based on the SC (Sub-Connected) structure, the design of analog precoding is done in the RF (Radio Frequency) domain, and then the low-dimensional digital precoder is used to utilize the equivalent channel, and the extent to which the spectral efficiency is affected by the number of overlapping antennas is analyzed, which achieves a good tradeoff between the system performance and the hardware cost [14]. Du, J et al. designed a hybrid precoding based on channel correlation codebook and the optimized analog and digital precoding matrices showed significant improvement in spectral performance compared to the hybrid precoding matrix based on random vectorized codebook, however, the method is energy inefficient as it compensates for the performance difference by increasing the energy consumption [15]. Although the hybrid precoding technique, which incorporates both digital and analog precoding, has the advantages of both schemes and can well equalize the energy efficiency and spectral efficiency of the system; however, the phase shifter in analog precoding, which imposes a limitation on the analog precoding matrix, increases the complexity of the precoder.

Therefore, current research in the field of precoding detection algorithms focuses on the design of hybrid precoders under constraints to maximize the optimization of algorithm performance and reduce the complexity of algorithm implementation. For example, Liu, F et al. proposed an adaptive sub-connected structure hybrid precoder for dynamic antenna array subset partitioning based on channel state information, where only a small number of phase shifters are used for each subset to connect all the RF links, and the optimization of the switching matrix of the phase shifters is implemented by an enumeration algorithm by adding a diagonal loading factor to the phase shifter matrix, which results in a good spectral efficiency and a low power consumption [16]. Zhang, F and Wu, M proposed a Threshold Orthogonal Matching Tracking Algorithm (TOMP) which, by setting a threshold value to the system, makes the system more spectrally efficient than the OMP algorithm and close in complexity to the optimal hybrid precoding algorithm [17]. Ding, Q et al. used a low-resolution digital-to-analog converter and an analog-to-digital converter to design a two-stage alternating optimized hybrid precoding scheme that achieves a balance between spectral and energy efficiencies with some reduction in complexity [18]. Mahmood, M et al. investigated a low-resolution phase shifter with fully adaptive subconnection hybrid precoding, in which the RF chain and inter-antenna connection states are dynamically controlled by switching matrices, converted the objective function maximization problem into a noncoherent combinatorial problem, and generated an approximate simulated precoding matrix by applying a cross-entropy optimization algorithm to update the probability mass of each element of the iterative simulated precoding matrix, and the experimental results showed that the hybrid precoding algorithm has high energy efficiency and low computational complexity [19]. Xie, T et al. derived the analog precoding matrix directly with the help of Orthogonal Matching Tracking (OMP) algorithm and then computed the digital precoding matrix by means of Mean Value Iteration algorithm, this method does not require Singular Value Decomposition (SVD) operation, which reduces the complexity of the implementation and improves the spectral efficiency of the system and reduces the BER [20]. Dai, L et al. proposed hybrid precoding algorithm under SC structure which uses an iterative approach which can achieve low complexity effect, it divides the antenna into multiple individual subarrays, transforms the optimization problem of the whole system into an optimization problem for each subarray, and eliminates the interference generated by the array antennas by using the serial interference method [21].

In practical communications, both non-circular and circular signals are frequently used signals, and the incident signals received by arrays often coexist with both. Therefore, it is

important to study the direction finding problem for coexistence of circular and non-circular signals in modern communication networks. To address such problems, Gupta, P and Agrawal, M proposed an improved nested array design that effectively increases the number of continuously available delay cells in the virtual array by dynamically adjusting the spacing between the dense and sparse subarrays and extending the sparse subarray internal array element spacing to enhance the estimation of noncircular signals [22]. Zhang, X proposed an algorithm for estimating the direction of arc (DOA) of mixed circular and noncircular signals based on nonuniform line arrays, which utilizes virtual array interpolation and kernel-paradigm minimization to reconstruct the augmented generalized covariance matrix and the augmented generalized nonconjugate covariance matrix by using the outputs of the difference array and and the co-array, respectively [23]. Tian, Y et al. proposed a multi-parameter estimation method for coherent distribution sources in the mixed case of circular and non-circular signals, which first constructs a perturbed paradigm minimization problem in a sparse representation framework, and then solves the problem through the joint use of the truncated L1-function approximation, the cost-function decomposition, and an iterative strategy, and finally estimates the multiple parameters by outputting sparse vectors [24]. Wan, L and Xie, L innovatively constructed three types of estimator frameworks according to the different characteristics of incident signals to categorize and estimate circular, maximally non-circularity and generally non-circularity signals, and then obtain the boda direction of the corresponding signals, which extends the applicability of the algorithms [25]. Teng, L et al. designed an enhanced sparse nested array structure for the challenge of mixing non-circular and circular signal scenarios, the core innovation of which lies in the complete elimination of hole defects from the virtual array by optimizing the physical array element arrangement, the method further combines with the virtual signal reconstruction technique of sum and difference co-array, and based on the theory of atomic paradigm minimization, it realizes the joint estimation of mixed-signal DOA without the need of mesh discretization [26]. Cai, J et al. investigated the problem of underdetermined DOA estimation for the mixing of circular and noncircular signals under sparse arrays, and proposed a compressed-aware DOA estimation algorithm that more efficiently exploits the degrees of freedom provided by the difference and sum covariance arrays generated by vectorization of covariance and pseudo-covariance matrices of the arrays [27].

In 5G evolutionary high concurrency scenarios, especially in high-frequency band applications such as 230 MHz, channel conditions are complex and interference is prominent. The research centers around the fusion of low-complexity precoding and non-circular signal detection to improve the performance of multiple-input multiple-output (MIMO) systems. It advances in two main directions, one is the originating optimization. Lattice-based approximation and ordering mechanisms are introduced to enhance precoding interference suppression. The lattice basis approximation (e.g., LLL algorithm) transforms the channel matrix into an approximately orthogonal basis, which significantly reduces the nearest point search complexity. It also draws on the sorting idea in V-BLAST to optimize the transmit order by row-column transformation, which further helps the system eliminate interference. Secondly, the receiving end is improved to enhance the linear detector performance by utilizing the non-circular characteristics of the signal. Modulated signals such as BPSK and ASK are typical non-circular signals, and their statistical properties are not symmetrically distributed. The study derives the extended ZF (EZF) and extended MMSE (EMMSE) detectors, which incorporate the noncircular information into the detection criterion by constructing the augmented receive vector.

2 Vector precoding and non-circular signal detection algorithms in highly concurrent MIMO systems

In high concurrency MIMO systems, spatial multiplexing techniques are often used to improve spectral efficiency and system capacity. In this section, the M_t -sending and M_r -receiving MIMO system is modeled and its signal representation and detection basis is given.

2.1 Modeling of spatially multiplexed MIMO systems

The spatially multiplexed MIMO system with M_t transmit, M_r receive, and M data streams transmitted in parallel is shown in Fig. 1.

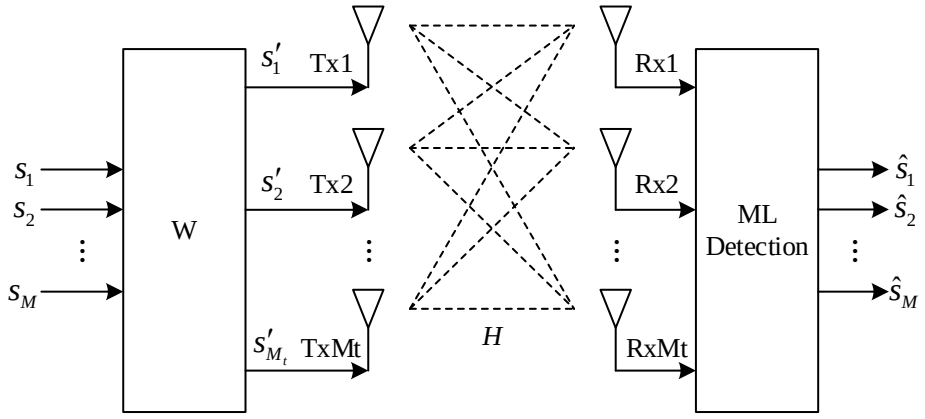

Figure 1: Space Multiplexing MIMO System Framework

In the downlink, there is typically $M_t \geq M_r$ and $M \leq M_r$ is typically set in order to make the transmitted signal separable at the receiving end. Let $s=[s_1, s_2, \cdots, s_M]^T$ be the symbol vector consisting of information symbols transmitted in the same time slot by M parallel data streams, with elements $s_i \in S, 1 \leq i \leq M$, and S being the set of modulated symbols normalized by the energy, then s the variance matrix is $R_{ss}=E\left\{ss^H\right\}=I_M$. The $W \in C^{M_t \times M}$ is a linear precoding matrix with the following energy constraint:

$$tr\left(WW^H\right)=M \tag{1}$$

where $tr(\cdot)$ denotes the trace of the matrix. The transmit symbol vector s is encoded by the precoding matrix W and the transmit signal vector is:

$$s'=\left[s'_1, s'_2, \cdots, s'_{M_t}\right]^T=Ws \tag{2}$$

$s'_i, 1 \leq i \leq M_t$ is the symbol transmitted on the ith antenna after precoding. Under a flat fading channel, the received signal vector $y \in C^{M_r \times 1}$ consisting of the signals on each receiving antenna of the linear precoded spatial multiplexing MIMO system is:

$$y = \sqrt{\frac{E_s}{M}} HWs + n \tag{3}$$

where E_s is the average signal energy per symbol period at the receiving antenna, $H \in C^{M_r \times M_t}$ is the MIMO channel transmission matrix; $n \in C^{M_r \times 1}$ is the white Gaussian noise vector and the variance matrix is $E\left\{nn^H\right\} = N_0 I_{M_r}$.

The receiver uses a maximum likelihood detection algorithm to recover the transmit signal vector, and its judgment symbol vector is the solution of the following equation:

$$\hat{s} = \arg\min_{s \in S} \left\| y - \sqrt{\frac{E_s}{M}} HWs \right\|_2 \tag{4}$$

where $\|\cdot\|_2$ is the 2-parameter of the vector.

For the channel matrix H, there is the following singular value decomposition:

$$H = U\Sigma V^H \tag{5}$$

where U and V are the You matrices of $M_r \times M_r$ and $M_t \times M_t$, respectively, which satisfy $UU^H = I_{M_r}$ and $VV^H = I_{M_t}$, and $\mathbf{\Sigma}$ is the singular value matrix of $M_r \times M_t$:

$$\Sigma = \left[\overline{\Sigma} \quad 0_{M_r \times (M_t - M_r)} \right] \tag{6}$$

$$\overline{\Sigma} = diag\left\{ \sigma_1, \sigma_2, \cdots, \sigma_{M_r} \right\} \tag{7}$$

where $\sigma_i \geq 0 \left(\sigma_i \geq \sigma_{i+1}, 1 \leq i \leq M_r \right)$ is the i th singular value of the channel matrix. Substituting Eq. (5) into Eq. (2) and left-multiplying the matrix U^H on both sides of Eq. (2) simultaneously gives:

$$\begin{aligned} y = U^H y &= \sqrt{\frac{E_s}{M}} U^H U \Sigma V^H W s + U^H n \\ &= \sqrt{\frac{E_s}{M}} \Sigma \tilde{s} + n = \sqrt{\frac{E_s}{M}} \overline{\Sigma} \tilde{s}_{M_r} + n \end{aligned} \tag{8}$$

where $y = [\tilde{y}_1, \tilde{y}_2, \cdots, \tilde{y}_{M_r}]^T$, $\tilde{s} = V^H W s$, $n = U^H n$, $\tilde{s}_{M_r} = [\tilde{s}_1, \tilde{s}_2, \cdots, \tilde{s}_{M_r}]^T$ is a vector consisting of the first M_r elements of $\tilde{s}$. In this way, the original MIMO system can be equated to the parallel subchannel transmission model shown in Fig. 2.

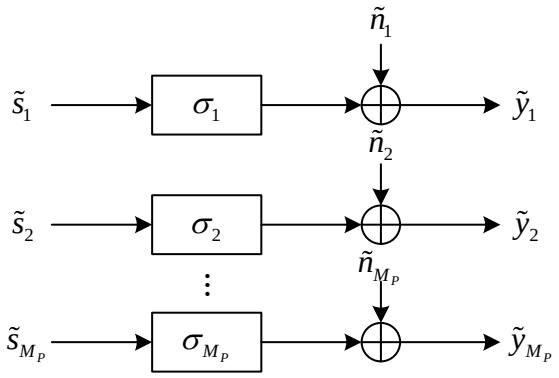

Figure 2: Sub-channel transmission model of spatial multiplexing MIMO system

2.2 Vector precoding algorithm

The main idea of vector precoding is a process of obtaining the precoding vector p by some specific algorithm and performing a nonlinear pre-equilibrium on the sum vector $(a+p)$ of the transmit signal vector a and the precoded vector p. The vector precoding is also known as SWC, which means that it is planned in an organized manner without being chaotic. The reason why the precoded vector p is said to be non-perturbative to the signal a is because of the process of modulo $\mathrm{mod}\, S_A(\cdot)$ operations at the receiver side, and since the precoded vector p has to satisfy $p \in AZ^k$, the result of the modal transformation for the vector p is a zero vector.

The basic framework of vector precoding according to the above idea is shown in Fig. 3 below:

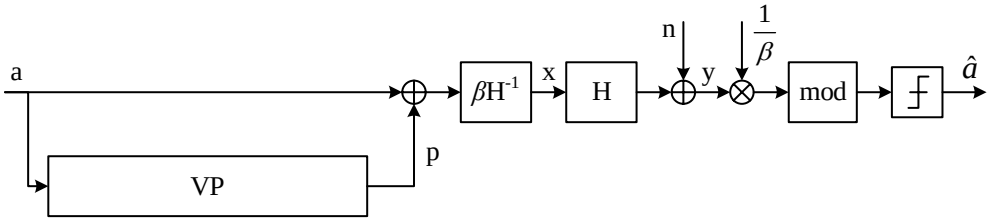

Figure 3: The basic framework of vector precoding

From the figure, it can be seen that if β is larger then the noise of the received signal at the receiving end is $\frac{1}{\beta}n$, and its value is smaller, and for the transmitted signal a an ideal pre-coding vector can always be found to maximize the scaling factor β.

Therefore usually the selection of the vector factor p in precoding is aimed at maximizing the scaling factor β so that the interference noise is minimized.

2.2.1 Fundamentals of vector precoding based on lattice decoding

If the signal is modulated with M-ary QAM modulation, then the amplitude of the modulated symbol is $\left[-\sqrt{M}/2, \sqrt{M}/2\right]$, defining $A=\sqrt{M}$. The received signal is:

$$\bar{y}_k = \mathrm{mod}\, s_A(y_k) \tag{9}$$

The ideal transmission precoded signal after linear pre-equalization is:

$$x = \beta H^{-1}(a + p) \tag{10}$$

where the effect of the vector signal p on the transmitted signal is eliminated at the receiving end by modulo arithmetic, since $p \in AZ^k$.

For the transmitted signal its transmitted power is constant and hence there is:

$$\varepsilon\left\{\|x\|^2\right\} = K\sigma_a^2 = const. = \beta^2 \varepsilon\left\{\left\|H^{-1}(a + p)\right\|^2\right\} \tag{11}$$

Since the emitted power is constant, to maximize the scaling factor β means to minimize this term $\left\|H^{-1}(a + p)\right\|$ and thus have:

$$P = \arg\min_{p \in AZ^k} \left\|H^{-1}(a + p)\right\|^2 \tag{12}$$

The receiver signal y is:

$$y = HH^{-1}(a + p) + \frac{1}{\beta} n \tag{13}$$

After performing the modulo operation, for $k = 1, ..., K$:

$$\begin{aligned} y_k &= \mathrm{mod}\, S_A(y_k) = \mathrm{mod}\, S_A\left(a_k + p_k + \beta^{-1} n_k\right) \\ &= \mathrm{mod}\, S_A\left(a_k + \beta^{-1} n_k\right) \end{aligned} \tag{14}$$

For the precoding vector p there is:

$$P = \arg\min_{p \in AZ^k} \left\|H^{-1}(a + p)\right\|^2 = \arg\min \left\|H^{-1}a + H^{-1}p\right\| \tag{15}$$

In this case, the process of solving for p is to search for the vector p in the lattice $AH^{-1}Z^k$ to the nearest distance to $H^{-1}a$. This method is also called vector precoding based on lattice decoding.

$$\beta = \sqrt{\frac{K\sigma_a^2}{\varepsilon\left\{\left\|H^{-1}(a + p)\right\|^2\right\}}} = \sqrt{\frac{K\sigma_a^2}{trace\left(X^T X\right)}} \tag{16}$$

The choice of β is related to the transmit power, if the precoding vector is $X = \left[x[0], \cdots, x[L_B - 1]\right]$, for the scaling factor β there:

$$\beta = \sqrt{\frac{KL_B\sigma_s^2}{trace\left(X^T X\right)}} \tag{17}$$

For signals with small dimensions the standard lattice decoding algorithms can be used for full search, especially the spherical decoding algorithm.

The vector precoding based on lattice decoding is shown in Figure 4 below:

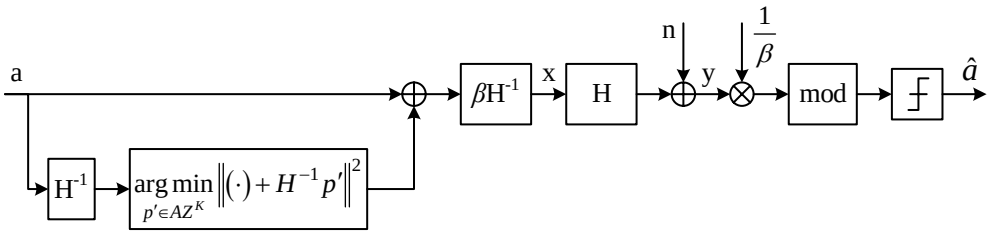

Figure 4: Vector precoding scheme based on trellis decoding

The nearest point search is used in lattice decoding to find the nearest vector p, where a spherical decoding algorithm based on the search for the nearest point is used.

2.2.2 Vector precoding based on lattice approximation assistance

In vector precoding based on lattice decoding, such as spherical decoding, the complexity increases rapidly with the increase of dimension K. Therefore, in order to simplify the complexity of the search operation, a simpler but effective vector precoding scheme - lattice simplification-based vector precoding, which is also an approximate nearest-point search method - is proposed.

When using the LLL algorithm for lattice approximation, the algorithm is only applied to real matrices.

This approximate nearest point search method is based on LLL approximation of the inverse matrix H^{-1} of the channel matrix, so that the approximated matrix has quasi-orthogonality, and the approximation basis of the approximated matrix H^{-1} is satisfied by $\overline{H_{red}}$:

$$\bar{H}_{red} = H^{-1}R \tag{18}$$

where $\bar{H}_{red}$ is the approximate matrix and R is the You array with $I = RR^{-1}$ and $\left|\det(R)\right| = 1$.

The approximate basis matrix $\bar{H}_{red}$ is a quasi-orthogonal matrix with better orthogonality and anti-interference properties than the inverse matrix of the channel matrix H^{-1}, so the approximate basis matrix is used here for the pre-coding process of the transmitted signal.

Due to its better orthogonality, the interference immunity of the signal sent through the wireless channel at the receiving end is better than that of the linear precoding directly with the inverse matrix H^{-1}. Although there is a certain loss of performance compared to the nearest-point searching algorithm based on the lattice decoding, the lattice approximation-assisted precoding algorithm greatly reduces the complexity of the computation, particularly when the number of transmitting and receiving antennas of the system is increased. If the lattice-aided algorithm is combined with V-BLAST, the precoding performance is very close to that of the lattice-based precoding algorithm.

The reason for the R matrix and the precoding vector p belonging to the integer domain is to restrict the search for the nearest vector to an integer domain, i.e., to a fixed lattice. This greatly simplifies the complexity of the search and finds the nearest vector quickly and more accurately.

If we introduce the quasi-orthogonal shortest approximation basis $\bar{H}_{red}$ and use a rounding approximation, then for $P = \arg\min_{p \in AZ^k} \left\| H^{-1}a + H^{-1}p \right\|^2$ in the precoding vector p can be approximated:

$$P_{approx} = -ARQ_{z^k}\left\{ \frac{1}{A}\bar{H}_{red}H^{-1}a \right\} = -RQ_{z^k}\left\{ R^{-1}a \right\} \tag{19}$$

Here $QA\{\ \}$ denotes $Q_{AZ}\{x\} = A\left\| \left[\frac{1}{A}x \right] \right\|$, which is defined for $\|[x]\|$ to be the point closest to an integer with respect to x, that is, $\|[x]\| = [x + 1/2]$, where $[x]$ denotes the largest integer that is smaller than x, and $\lceil x \rceil$ denotes the smallest integer that is larger than x.

Thus the precoded transmit signal is given by the following equation:

$$x = \beta H^{-1}\left(a - RQ_{Az^k}\left\{ R^{-1}a \right\} \right) \tag{20}$$

If the V-BLAST algorithm is combined with the lattice simplification method, the performance of the precoding system can be greatly improved, and the optimal precoding order can be achieved by sorting to increase the anti-interference ability.

According to the idea of V-BLAST detection, the best precoding order can be obtained by performing a determinant transformation on the channel matrix $\bar{H}_{red}$. This can be obtained:

$$B = F\bar{H}_{red}P \tag{21}$$

Here $B = [bkl] \in R^{K \times K}$ is the lower triangular matrix whose diagonal is the unit element, defined:

$$\begin{cases} b_{kl} = 1 & k = l \\ b_{kl} = 0 & k < l \end{cases} \tag{22}$$

$F \in R^{K \times K}$ is a row orthogonal matrix, and P is a $K \times K$ permutation matrix identifying the best order in V-BLAST. Definition:

$$q = -FH^{-1}a \tag{23}$$

$$\tilde{q}_1 = q_1 \tag{24}$$

For $k = 2, ..., K$ has

$$\tilde{q}_k = Q_{AZ}\left\{ q_k - \sum_{l=1}^{k-1} b_{k,l}\tilde{q}_l \right\} \tag{25}$$

Note that $Q_{AZ}\{x\} = A\left\lfloor \frac{1}{A}x \right\rfloor$

This results in an approximate point precoding vector:

$$P_{approx} = RPq \tag{26}$$

2.3 MIMO Detection Algorithm Based on Noncircular Characteristics of Transmitted Signal Sources

In addition to precoding techniques, exploiting the noncircular characteristics of signals can also significantly improve the detection performance of MIMO systems. In this section, extended detectors are proposed for non-circular signals.

2.3.1 Generalized algorithms

The following assumptions are used in this paper:

(1) The emitted signal x is non-circular;

(2) $E\left[xx^H \right] = PI_{N_x}$;

(3) $E\left[ww^H \right] = \sigma^2 I_{N_x}$;

(4) $E\left[wx^H \right] = 0$;

(5) The channel is quasi-static.

Let $x = x(t), y = y(t), w = w(t)$, which leads to:

$$y = \begin{bmatrix} y(t) \\ y^*(t+\tau) \end{bmatrix} = \begin{bmatrix} Hx(t) \\ H^* x^*(t+\tau) \end{bmatrix} + \begin{bmatrix} w(t) \\ w^*(t+\tau) \end{bmatrix} \tag{27}$$

An estimate of x can be derived from y by using the following equation:

$$x = Cy \tag{28}$$

$$C = E\left[xy^H \right]\left(E\left[yy^H \right] \right)^{-1} \tag{29}$$

2.3.2 Expanding the ZF Detector

The real signal (BPSK or ASK signal) is a typical non-circular signal, then equation (27) can be expressed as:

$$y = Hx + w \tag{30}$$

In the formula: $H = \left[H^T \; H^{*T} \right]^T$; $w = \left[w^T \; w^{*T} \right]^T$. The transmitted signal x can be estimated by the ZF receiver, where:

$$x_{EZF} = C_{EZF}\, y \tag{31}$$

where $C_{EZF} = H^{\dagger\dagger}$. Since the linear space under consideration has been extended to the $N_T \times 2N_R$ dimensional space, the method is referred to as Extended ZF (EZF) to differentiate it from conventional ZF.

For the ZF detector, the estimate $\hat{x}_{xxr}$ in Eq. (31) can be expressed as:

$$x_{xxr} = x + H^{\dagger} w \tag{32}$$

where $H^{\dagger} w$ is the interference at the output of the EZF detector.

For the real signal x, it follows:

$$E\left[\left\|x_{xxr} - x\right\|^2\right] \le \frac{1}{2} E\left[\left\|x_{xr} - x\right\|^2\right] \tag{33}$$

By utilizing the non-circular characteristic, the interference energy is reduced to less than half. This results in a significant improvement in bit error rate (BER) performance relative to conventional ZF.

2.3.3 Expanding the MMSE Detector

This part is a specific case of the real signal in Eq. (29) when $\tau = 0$. The detector in Eq. (29) can be written as:

$$C_{EMMSE} = P H^{H} R^{-1} \tag{34}$$

Eq.

$$R = E\left[\, y y^{H} \right] \tag{35}$$

The signal vector x is estimated:

$$x_{EMMSE} = C_{EMMSE}\, y \tag{36}$$

In this paper, we refer to this method as extended MMSE (EMMSE).

Let x be a noncircular signal and x be the estimate of x derived based on the algorithm described in (28), with:

$$E\left[\left\|x - x\right\|^2\right] \le E\left[\left\|x_{mmse} - x\right\|^2\right] \tag{37}$$

If x is real, then the proposed algorithm is an extended MMSE with:

$$E\left[\left\|x_{EMMSE} - x\right\|^2\right] < \frac{1}{2} E\left[\left\|x_{zr} - x\right\|^2\right] \tag{38}$$

2.3.4 Optimality discussion

(1) Optimality of ML: Conventional MMSE and conventional ZF are improved by exploiting the noncircularity property, but Eq. (30) shares the same ML solution, and thus the optimal system performance remains the same.

(2) Sub-optimality of EMMSE: In a frequency-flat single-input/single-output (SISO) system, there is almost no difference in the BER performance of ML, MMSE, and ZF detectors because both MMSE and ZF can be reduced to ML algorithms. For the frequency-flat SIMO system, the maximum ratio combining (MRC) and ML have the best performance, and the noncircular maximum likelihood sequence estimation (NCIR-MLSE) receiver also achieves the best performance in a linear interference background. However, the situation is different for frequency-flat MIMO systems even if the signal x is linear. The SIMO system can be written as:

$$y = h_i x_i + v_i \tag{39}$$

where $v_i = \sum_{n \neq i}^{N_t} h_n x_n + w$, and the EMMSE solution of x is the suboptimal solution of the system. Therefore, the EMMSE is the suboptimal detector compared to the ML method.

3 Non-circular signal detection low-complexity precoding performance testing experiments

The above describes a low-complexity algorithmic framework that combines lattice-approximate precoding and non-circular signal detection, and theoretically demonstrates its performance in highly concurrent MIMO systems. In this chapter, a series of simulation experiments are conducted to evaluate the performance of the algorithm from three dimensions in a high concurrency environment in the 230MHz band. Firstly, the BER performance of the precoding scheme combining lattice approximation and V-BLAST at the transmitter side is verified; based on this, the perspective is shifted to the receiver side, focusing on the reachability and computational complexity of the non-circular extended detector in real multi-user scenarios; and further exploring the boundaries of the extended detector under the constraints of different strengths of scattering noises and antenna layouts.

3.1 Vector precoding performance validation

Firstly, to explore the performance of the hybrid precoding structure with lattice-approximate simplex + V-BLAST ordering proposed in this paper in real wireless transmission, this section constructs a MIMO system model with M_t transmit and M_r receive based on the Matlab simulation platform to simulate the high-interference, multiuser concurrent scenarios in the 230 MHz frequency band.

Conventional linear precoding (ZF), lattice-based simple precoding (LLL) and lattice+ V-BLAST ordering are selected for the experiments.

3.1.1 Performance comparison of different coding methods under 2×2

Fig. 5 shows the comparison of the BER performance of three different precoding methods under slow fading channel conditions with two transmitters and two receivers (2×2MIMO),

normalized power at the transmitter side, and the best channel quality, under 16QAM system conditions.

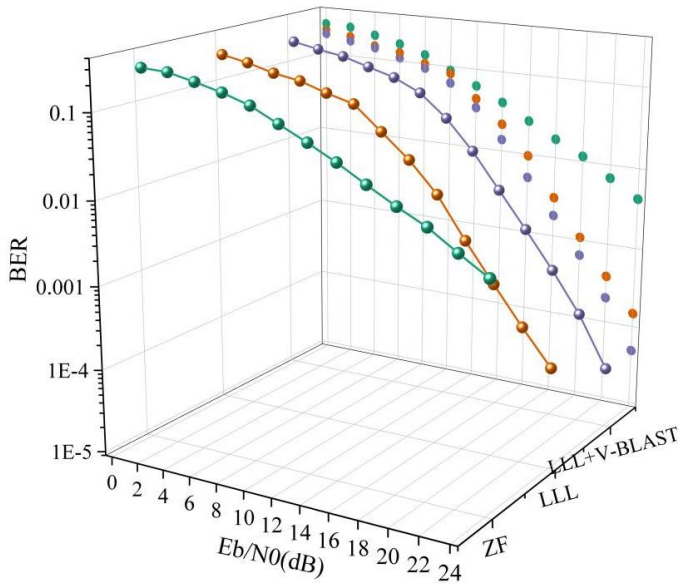

Figure 5: Performance of different encoding methods in 2×2 configuration

When the BER is 0.01, linear precoding requires close to 20dB SNR to achieve it, whereas vector precoding based on Gerber-assisted precoding reduces the BER to 0.001 at about 16dB. With the integration of the V-BLAST sequencing algorithm, the algorithm achieves a BER as low as 0.01 at only about 14dB, and at 16dB it reaches 5.1E-3. Taking BER=0.01 as a threshold, Gerber+V-BLAST saves about 4-6dB of power compared to linear precoding.

Further observing the overall trend, the performance gap between the three schemes gradually widens as the signal-to-noise ratio increases. In the middle and high SNR above 12dB, the advantage of GEOJUNCT+V-BLAST becomes more and more obvious. At 12dB, its BER is only 0.0325, while linear precoding has 0.0615, almost double the difference. This indicates that in the environment with better signal quality, the interference elimination effect brought by the joint optimized sequencing and lattice-based approximation is more prominent.

3.1.2 Performance comparison of different channel qualities under 2×2

The above experiments are carried out under the best channel quality, in order to explore the impact of different signal quality on the BER performance of the precoding algorithm, the experiments are set under three conditions of channel quality p=1, p=0.5 and p=0 respectively, and the results of the experiments are shown in Fig. 6.

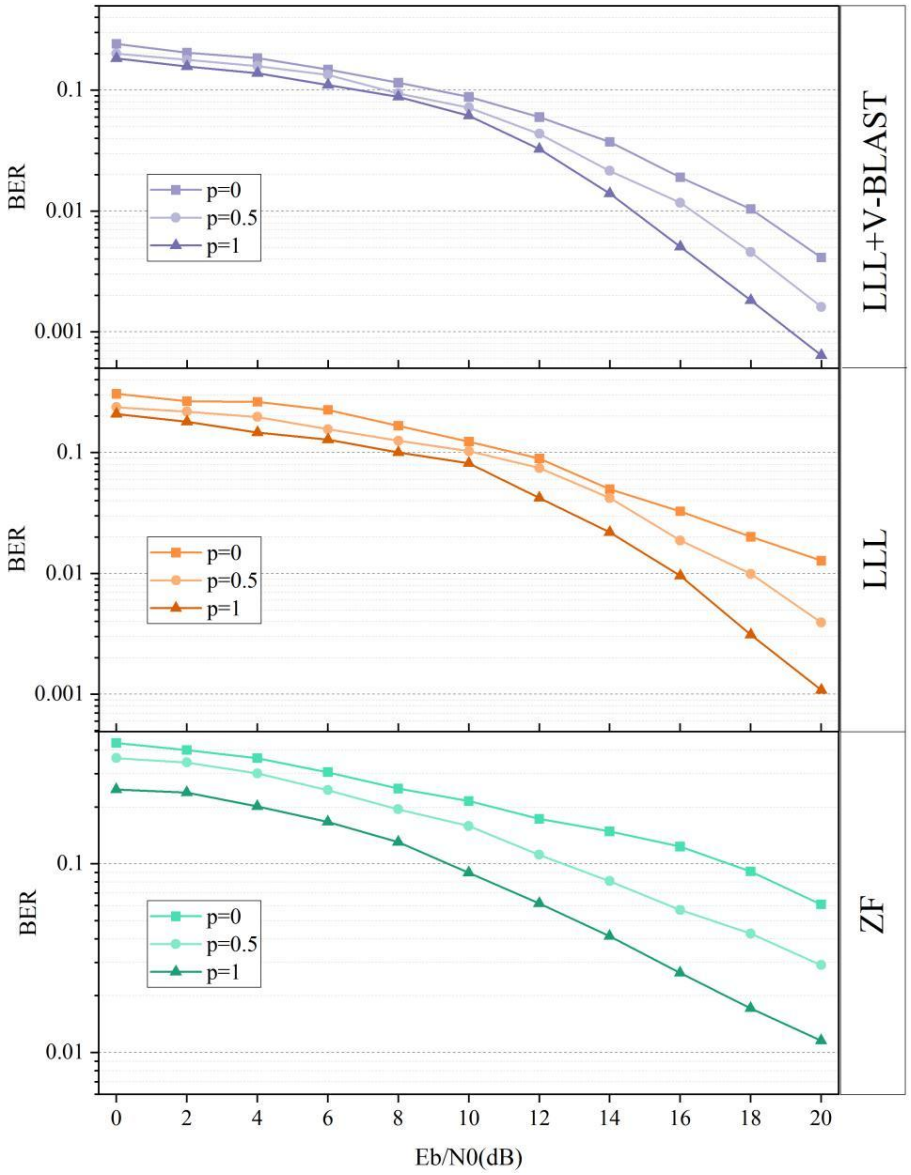

Figure 6: Comparison of different channel quality performances

Continuing with the 12 dB SNR example, when the channel quality is the best (p=1), the BER is only 0.0325 for Gergely Simplex+V-BLAST and 0.0615 for linear precoding; when the channel quality is compromised (p=0.5), both rise to 0.0435 and 0.1114, respectively; and at the worst quality (p=0), the BER improves to 0.0598 and 0.1726.Clearly, channel quality degradation affects all schemes, but the degradation is much slower for Gjørn + V-BLAST, which still maintains relatively good availability in poor channels.

On the contrary, if BER = 0.05 is used as the criterion, under the ideal channel with p = 1, linear precoding requires 10-12 dB SNR, while the Gergely Simplified + V-BLAST in this paper only requires about 8 dB; under the poor channel with p = 0, linear precoding is difficult to reach the criterion even up to 20 dB, and the BER is still 0.0609, which fuses the V -BLAST lattice simple precoding can be realized at around 15dB.

3.1.3 Performance comparison of different coding methods under 4×4

Further, different precoding algorithms are tested under 4-transmitter-4-receiver (4×4MIMO) conditions and the experimental results are shown in Fig. 7.

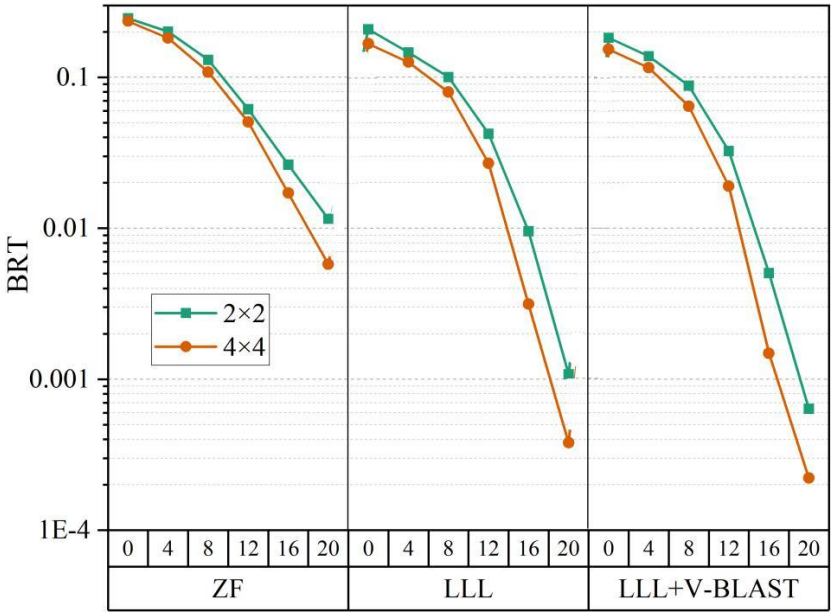

Figure 7: Performance of different encoding methods in 4×4 configuration

The algorithm performance of each scheme is improved under 4×4MIMO conditions than under 2×2, and the improvement is more obvious at high SNR. At SNR = 12 dB, the BER of Gerber+V-BLAST is 0.0325 in the 2×2 configuration; it drops to 0.0190 in 4×4 MIMO, a decrease of about 42%. In comparison, linear precoding drops from 0.0615 to 0.0506, a reduction of only about 18%.

When focusing on the difference in the required SNR at the same BER level, e.g., to achieve a BER ≈ 0.01, in a 2-transmitter-2-receiver system, GEO+V-BLAST needs about 16 dB, while linear precoding needs close to 20 dB, and in a 4×4 system, the former needs only about 14 dB, while the latter still needs 17 dB. More antennas bring spatial diversity gain, and GEO+V-BLAST can be used for this purpose through the V-BLAST makes full use of the structural gain brought by multiple antennas through inverse matrix processing of the channel, thus realizing higher spectral efficiency and power utilization.

3.2 Pre-coded user reachable rate and complexity

Continuing with the measurement of different precoding schemes, this section also introduces the classical algorithm Spherical Decoding (SD) for Lattice Decoding precoding, and the average user reachable rate and complexity of the four different precodings are shown in Fig. 8 under the environmental conditions of the number of antennas N=128 and cell users K=300 with the selected SNRs of 10 and 20 dB.

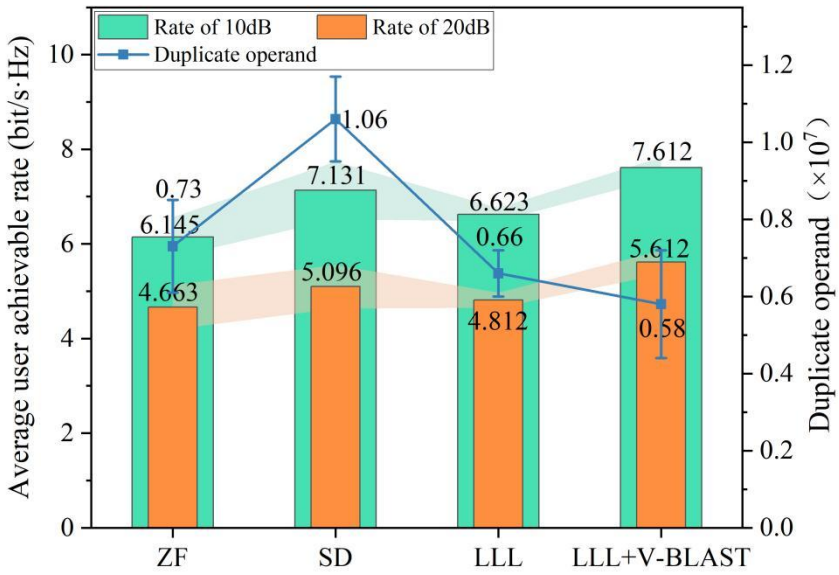

Figure 8: Average user achievable rate and complexity of different precoding schemes

As a benchmark, the linear precoding ZF has an average user-reachable rate of 6.145 bit/s/Hz at 10 dB SNR and a computational complexity of 0.73×10^7. When the lattice decoding vector precoding based on spherical decoding is introduced, its rate is increased to 7.131 bit/s/Hz by searching for the nearest point, but at the same time its complexity increases to 1.06 × 107 complex operations with the increase of the number of dimensions. In this regard, Lattice Lumped Simplification (LLL) is introduced to improve the channel matrix orthogonality and its complexity is reduced to 0.66×10^7. However, it incurs some loss in the process, which causes another slight decrease in the rate. This is then combined with V-BLAST intelligent sorting, and its performance is further enhanced, with the complexity further reduced to 0.58 × 107, and the user rate is increased to 7.612 bit/s/Hz at 10 dB SNR, which is a gain of 23.9% compared to the simple linear precoding, and also a 14.9% improvement over the LLL precoding.

3.3 Evaluation of non-circular extended detector performance

The superiority of the lattice simplex + V-BLAST vector precoding algorithm was verified above for the transmitter side, and we now turn to the study of low-complexity precoding detection algorithms for non-circular signals at the receiver side.

3.3.1 Space channel sensitivity studies

Firstly, based on the two precoding schemes of extended ZF and extended MMSE proposed in the study, a comparison is made with the original ZF and MMSE as well as the optimal detector ML.

The number of antennas equipped at the base station end of a cellular cell is considered to be 128, 256, and 5-140, and the overload factor β is chosen to be 0.1-2.5. In order to visualize the sensitivity of the above signal detection schemes to spatially correlated channels, the study sets different overload factors to observe the rates under different detection schemes. The number of antennas N is 128, the SNR is taken as 12 dB, and the variation of system and rate with β is shown in Fig. 9. (Since the study focuses on examining the EZF, EMMSE is improved by utilizing the non-circular characteristics, 3 more iterations of experiments are conducted for EZF and EMMSE.)

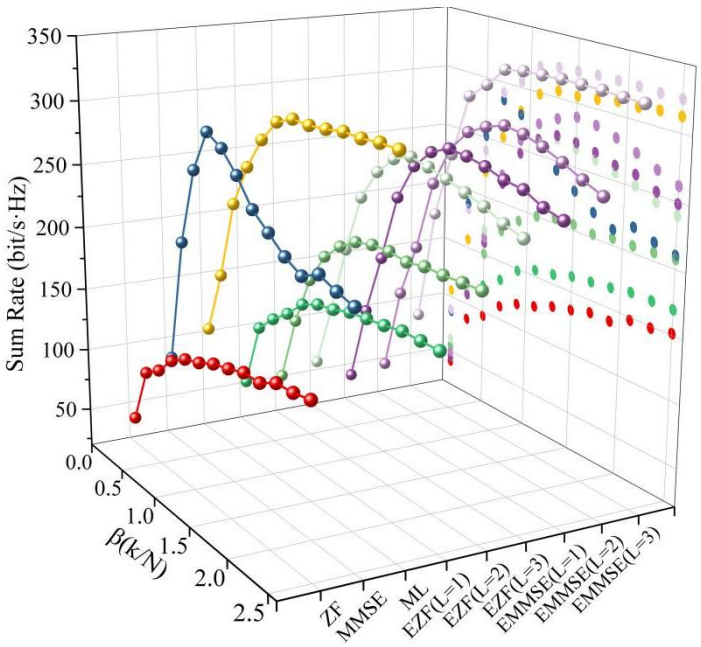

Figure 9: The system and rate change with the variation of the overload factor β

The precoding scheme that extends the MMSE linear detector increases the rate dramatically through iterations. For the original MMSE detector, it performs well with a small overload factor, but its rate decreases substantially as the number of users increases. Taking the data with overload factor β = 1.5 (when the number of users is 278) as an example, the ZF and MMSE precoding rates at this point are 154 and 216 bit/s/Hz, respectively, while the total precoding rate under the optimal ML detector is 331 bit/s/Hz. the EZF reaches 263 at the third iteration, which is also only 79% of the ML performance. Looking closely at the three green curves in the figure, the EZF performance still gradually improves through the iterations. Focusing on the purple curve of EMMSE, its rate after the first iteration has reached 283, which is 85% of the ML performance; the second iteration has improved to 325, which is close to the optimal ML performance; and the rate after the third iteration has reached 341, which is more than the ML. It is shown that the expanded MMSE precoding makes full use of its statistical properties for non-circular signals, and gradually learns and eliminates the special interference structure introduced by the non-circular characteristics of the signals through iterations.

3.3.2 Comparison of program rates for different base station days

The system and rate of various signal detection schemes with different number of base station antennas are also compared. The simulation parameters are set to SNR=12dB and the overload factor β is taken as 1.5.The variation of system and rate with the number of base station antennas N for different iterative detection schemes is shown in Fig. 10.

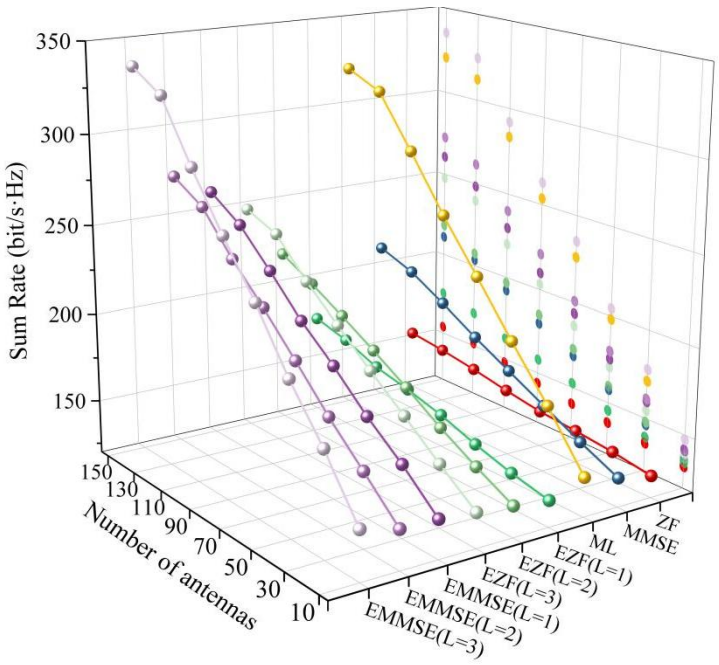

Figure 10: The variation of rate of different number of antennas under iterations

The rate under different detection schemes is almost positively linear with the increase of the number of antennas, when the number of antennas are all 10, the gap between the schemes is not large, and the gap between the schemes is gradually widened as the number of antennas keeps increasing. When increasing to 128 antennas, the optimal ML detector rate is 312 bit/s-Hz, and the EMMSE of 3 iterations reaches 325, and the lead is extended to 4.7%, which is consistent with the above experiment. However, at this time, as the number of antennas increases again to 150, the rate growth trend is slowed down, and the slope is obviously smaller, and the EMMSE (L=3) under N=150 is 335bit/s-Hz, which is only increased by 10 units, which is much lower than the previous increase of 29 units when the antenna N=90→110. It suggests that 128 antennas may be a beneficial inflection point for system configuration in practical 230 MHz massive MIMO system design. As the number of antennas continues to increase, the guide frequency overhead increases, the channel estimation error accumulates, and the marginal benefit diminishes.

3.4 Practical Performance Verification of Expanded Detectors in Multiple Noise Environments

To further analyze the practical performance of the extended ZF and extended MMSE detectors, the experiments are continued in a low-complexity MIMO system with highly concurrent 239 MHz band non-circular signals, and the actual and theoretical values of BRT BERs of different detectors are compared for different PD spacings with different transmit powers by taking the scattering noise ξ^2=0, 5 and 10 dB. Fig. 11 and Fig. 12 show the BER of different precoded detection schemes for PD spacing of d=0.2 and d=0.8, respectively.

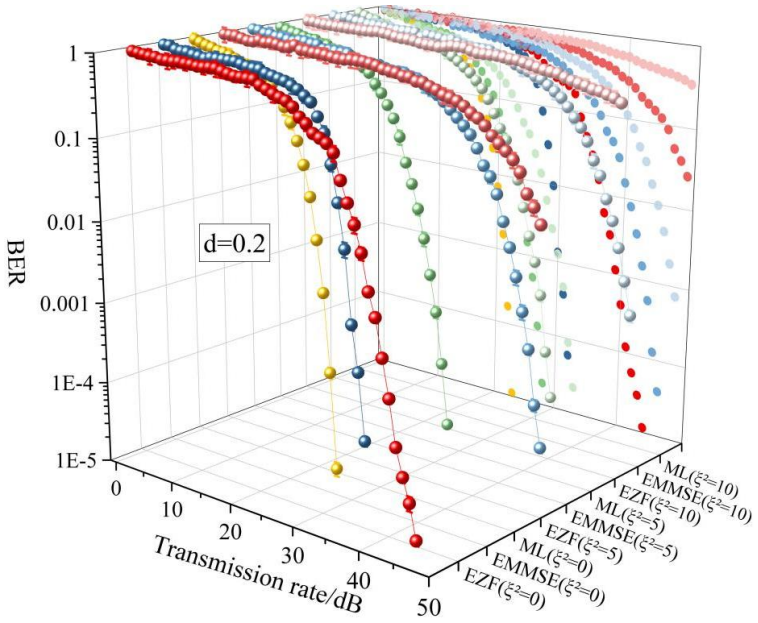

Figure 11: Bit error rates under different detection schemes of d = 0.2

The system is particularly sensitive to noise at the smaller spacing of d = 0.2. Continuing with BER = 0.01, the ML detector requires roughly 15 dB of transmit power to reach the threshold in the absence of scattering noise ($\xi^2 = 0$), while EMMSE requires about 18 dB and EZF nearly 20 dB. However, as the scattering noise is enhanced up to $\xi^2 = 10$ dB, the power required to reach the same BER threshold is significantly increased, and the performance loss starts to deteriorate: the performance loss reaches 19 dB for ML, 21 dB for EMMSE, and more than 23 dB for EZF. 19dB for ML, 21dB for EMMSE, and more than 23dB for EZF, indicating that in the spacing-constrained scenario with significant interference, while the ML optimality is still maintained, the advantage of EMMSE over EZF is even more prominent, as its required signal-to-noise is about 2-3dB lower than that of EZF on average, which shows better noise robustness, and once again demonstrates its suboptimality.

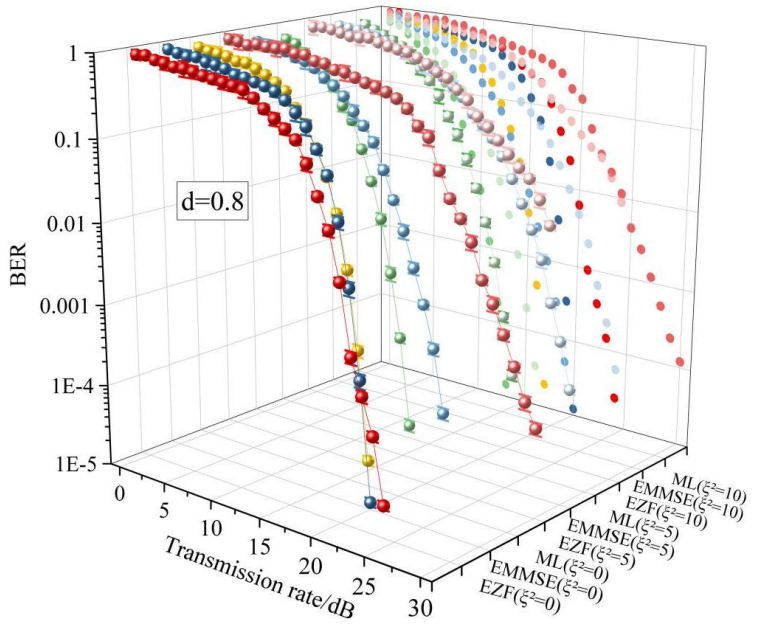

Figure 12: Bit error rates under different detection schemes of d = 0.8

When the PD spacing is increased to d=0.8, the performance improvement is significant. Also under the noiseless condition reaching BER=0.01, the ML, EMMSE, and EZF transmit power require 13dB, 16dB, and 18dB, respectively. when the scattering noise is increased to ξ^2=10dB, the three require 17dB, 19dB, and 21dB, respectively. the comparison reveals that increasing the spacing shifts the operating point of all the detectors under the same noisy condition towards a lower signal-to-noise ratio by about 2-4 dB, which is due to the fact that as the PD spacing increases, the optical channel correlation becomes smaller, the transmit power required to discriminate between different transmit LEDs becomes smaller, and the BER performance becomes stronger.

In addition, the difference error between the theoretical values and the actual values obtained from the simulation experiments in both figures is very small, and the error between the two is almost negligible in the figure. It shows the correctness of the theoretical derivation and analysis, which again confirms the optimality of ML and the suboptimality of EMMSE. Therefore, in the actual 230 MHz high concurrent system design, if the antenna layout allows, a larger PD spacing should be prioritized to obtain the spatial gain.

4 Conclusion

In this paper, the combination of transmitter-side precoding optimization and receiver-side detection enhancement is data-verified to be effective in improving system rate and reducing BER, providing a feasible path for 230MHz high concurrency MIMO system that combines high performance, low complexity and strong robustness.

Under 4×4 antenna configuration, the BER of GEOJAN+V-BLAST can be as low as 0.02 at 12dB SNR, which is more than 60% lower than 0.05 of linear precoding. When the channel quality factor p=0.5, the BER of this scheme at the same SNR is still about 50% lower than that of linear precoding, which demonstrates good environmental adaptability. Compared with the nearest-point search algorithm based on lattice decoding or simple lattice approximation algorithm, LLL+V-BLAST finds the optimal balance between performance and computational complexity with a complexity of 0.58×107 and a user-reachable rate of 7.612 bit/s/Hz at a signal-to-noise ratio of 10 dB. The EMMSE detector based on non-circular signal characteristics at the receiver side is closer to ML with a performance deterioration of 2 dB slower than EZF under scattering noise with ξ^2 = 10 dB.

Funding

This work was supported by State Grid Hebei Electric Power Co., Ltd. Technology Project "Research and Verification of High-Concurrency, Low-Power-Consumption Overlimit Communication Technology Based on 230MHz" (Project ID: kjcb2024-026).

References

[1] Shao, W., Ling, Z., Li, J., Lu, Y., Bai, W., & Zhang, D. (2019, May). Evolution trend of lte 230mhz electric wireless private network technology. In 2019 IEEE International Conference on Energy Internet (ICEI) (pp. 591-595). IEEE.

[2] Zhou, Z., Wang, L., Song, C., Shen, Y., Li, M., & Liu, S. (2024, May). Challenges of Data Consistency in High-Concurrency Environments: Algorithms and Implementation for the Electric Power Industrial Internet Platform. In 2024 5th International Conference on

Information Science, Parallel and Distributed Systems (ISPDS) (pp. 526-530). IEEE.

[3] Deng, X., Wu, Q., Ma, T., Gu, Z., & Deng, J. (2024, December). Optimization Method for Safe Operation of Distribution Network in Large-Scale and High-Concurrency Scenario. In Proceedings of the 2024 International Conference on Big Data Mining and Information Processing (pp. 91-96).

[4] Gong, J., Suo, S., Zhang, M., Jia, Y., & Liu, S. (2024, December). High Concurrent Data Transmission and Fault Tolerance Mechanism in Power Carrier Communication System. In 2024 IEEE 7th International Conference on Automation, Electronics and Electrical Engineering (AUTEEE) (pp. 1011-1016). IEEE.

[5] Cuomo, F., Campo, M., Caponi, A., Bianchi, G., Rossini, G., & Pisani, P. (2017, October). EXPLoRa: Extending the performance of LoRa by suitable spreading factor allocations. In 2017 IEEE 13th international conference on wireless and mobile computing, networking and communications (WiMob) (pp. 1-8). IEEE.

[6] Reynders, B., Wang, Q., Tuset-Peiro, P., Vilajosana, X., & Pollin, S. (2018). Improving reliability and scalability of LoRaWANs through lightweight scheduling. IEEE Internet of Things Journal, 5(3), 1830-1842.

[7] Gamage, A., Liando, J., Gu, C., Tan, R., Li, M., & Seller, O. (2023). LMAC: Efficient carrier-sense multiple access for LoRa. ACM Transactions on Sensor Networks, 19(2), 1-27.

[8] Lyu, J., Yu, D., & Fu, L. (2020, February). Achieving max-min throughput in LoRa networks. In 2020 International Conference on Computing, Networking and Communications (ICNC) (pp. 471-476). IEEE.

[9] El-Aasser, M., Elshabrawy, T., & Ashour, M. (2018, December). Joint spreading factor and coding rate assignment in LoRaWAN networks. In 2018 IEEE global conference on internet of things (GCIoT) (pp. 1-7). IEEE.

[10] Kouvelas, N., Rao, V., & Prasad, R. R. (2018). Employing p-CSMA on a LoRa network simulator. arXiv preprint arXiv:1805.12263.

[11] Shaban, A. W., Damen, O., Xin, Y., & Au, E. (2020). Statistically-aided codebook-based hybrid precoding for millimeter wave channels. IEEE Access, 8, 101500-101513.

[12] Dai, L., Gao, X., & Wang, Z. (2015, September). Energy-efficient hybrid precoding based on successive interference cancelation for millimeter-wave massive MIMO systems. In 2015 Radio and Antenna Days of the Indian Ocean (RADIO) (pp. 1-2). IEEE.

[13] Cui, M., & Zou, W. (2019). Low complexity joint hybrid precoding for millimeter wave MIMO systems. China Communications, 16(2), 49-58.

[14] Guo, Y., Li, L., Wen, X., Chen, W., & Han, Z. (2017, October). Sub-array based hybrid precoding design for downlink millimeter-wave multi-user massive MIMO systems. In 2017 9th International Conference on Wireless Communications and Signal Processing (WCSP) (pp. 1-4). IEEE.

[15] Du, J., Xu, W., Shen, H., Dong, X., & Zhao, C. (2018). Hybrid precoding architecture for massive multiuser MIMO with dissipation: Sub-connected or fully connected structures?. IEEE Transactions on Wireless Communications, 17(8), 5465-5479.

[16] Liu, F., Bai, X., Shi, H., Du, R., & Liu, H. (2020, August). Hybrid precoding with adaptive sub-connected architecture for mmWave massive MIMO systems. In 2020 IEEE 31st Annual International Symposium on Personal, Indoor and Mobile Radio Communications (pp. 1-6). IEEE.

[17] Zhang, F., & Wu, M. (2017, October). Hybrid analog-digital precoding for millimeter wave MIMO Systems. In 2017 IEEE 17th international conference on communication technology (ICCT) (pp. 69-73). IEEE.

[18] Ding, Q., Deng, Y., & Gao, X. (2019). Spectral and energy efficiency of hybrid precoding for mmWave massive MIMO with low-resolution ADCs/DACs. IEEE Access, 7, 186529-186537.

[19] Mahmood, M., Koc, A., & Le-Ngoc, T. (2021). Energy-efficient MU-massive-MIMO hybrid precoder design: Low-resolution phase shifters and digital-to-analog converters for 2D antenna array structures. IEEE Open Journal of the Communications Society, 2, 1842-1861.

[20] Xie, T., Dai, L., Gao, X., Shakir, M. Z., & Li, J. (2018). Geometric mean decomposition based hybrid precoding for millimeter-wave massive MIMO. China Communications, 15(5), 229-238.

[21] Dai, L., Gao, X., Quan, J., & Han, S. (2015, June). Near-optimal hybrid analog and digital precoding for downlink mmWave massive MIMO systems. In 2015 IEEE International Conference on Communications (ICC) (pp. 1334-1339). IEEE.

[22] Gupta, P., & Agrawal, M. (2018). Design and analysis of the sparse array for DOA estimation of noncircular signals. IEEE Transactions on Signal Processing, 67(2), 460-473.

[23] Zhang, X., Zheng, Z., Wang, W. Q., & So, H. C. (2022). DOA estimation of mixed circular and noncircular sources using nonuniform linear array. IEEE Transactions on Aerospace and Electronic Systems, 58(6), 5703-5710.

[24] Tian, Y., Yue, H., & Rong, X. (2020). Multi-parameters estimation of coherently distributed sources under coexistence of circular and noncircular signals. IEEE Communications Letters, 24(6), 1254-1257.

[25] Wan, L., & Xie, L. (2016, March). An improved DOA estimation algorithm for circular and non-circular signals with high resolution. In 2016 IEEE International Conference on Acoustics, Speech and Signal Processing (ICASSP) (pp. 3051-3055). IEEE.

[26] Teng, L., Wang, Q., Chen, H., Zhu, W. P., Liu, W., & Cai, J. (2020, June). DOA estimation for coexistence of circular and non-circular signals based on atomic norm minimization. In 2020 IEEE 11th Sensor Array and Multichannel Signal Processing Workshop (SAM). IEEE.

[27] Cai, J., Wu, B., Li, P., & Liu, W. (2017, October). A sparse representation based DOA estimation algorithm for a mixture of circular and noncircular signals using sparse arrays. In 2017 IEEE International Conference on Signal Processing, Communications and Computing (ICSPCC) (pp. 1-5). IEEE.